New synthesis of pure orthorhombic Mo-V-A oxide phases, where A = Sb, Bi and Pb, and testing for the oxidation of light alkanes

T. Le, R. Checa, P. Bargiela, M. Aouine, J. Millet

New synthesis of pure orthorhombic Mo-V-A oxide phases, where A=Sb, Bi and Pb, and testing for the oxidation of light alkanes.

T.M.N Le, R. Checa, P. Bargiela, M. Aouine and J.M.M. Millet*

Univ. Lyon, Université Claude Bernard Lyon 1, CNRS, IRCELYON - UMR 5256, 2 Av. Albert Einstein, 69626 Villeurbanne (France)

* Corresponding author: jean-marc.millet@ircelyon.univ-lyon1.fr

ABSTRACT

A new, microwave-assisted technique has been developed for the synthesis of microporous vanado-molybdate catalysts with an M1-type orthorhombic structure. This method allows various cations such as Sb, Bi and - for the first time - Pb, to be introduced into the hexagonal channels of the structure, without using any expensive structure directing agent. The influence of the aforementioned elements with lone pairs of electrons on the framework structure has been studied, and the crystalline structure of the Pb-containing phase was refined using the Rietveld method and powder diffraction data. The structure determination data are in good agreement with those obtained by different analytical or spectroscopic techniques. The catalytic properties of the catalysts have been determined for the oxidative dehydrogenation of ethane, and for the oxidation of propane into acrylic acid.

KEYWORDS: Crystalline Mo-V-O catalysts, selective oxidation, antimony, bismuth, lead, M1 phase, structure-activity relationship

1. Introduction

Multi-element molybdate mixed-oxide catalysts are among the most sophisticated catalytic oxidation systems ever discovered [1, 2]. The active phase of these catalysts, referred to as the M1 phase, is a complex solid solution with a bronze-type structure, made of $\{(M)M_5\}$ columns, where M=Mo, V (and possibly Nb or Ta), and comprising a stack with a central MO_7 bi-pyramid, surrounded by 5 edge-sharing MO_6 octahedra. These columns, which are connected to each other by corner-sharing MO_6 octahedra, form heptagonal and hexagonal channels running parallel to the columns [3, 4]. There are numerous ways for the composition of this phase to be varied, in terms of the nature of the constituent elements, and their relative contents. Nevertheless, for catalytic applications the octahedral network of the structure contains mainly Mo and V, and possibly small amounts of Nb or Ta cations. The hexagonal channels also need to be partially occupied by oxygen and Te or Sb cations, in cases where the process involves the oxidation or ammoxidation of propane [5-8]. The heptagonal channels are empty. Attempts to substitute the Mo and V cations with other elements were unsuccessful, except for the case of W, although no beneficial effect was observed in terms of the catalytic oxidation properties [9, 10]. Elements with lone electron pairs, such as Te or Sb, have been shown to be essential for the oxidation of propane, in particular for the removal of α-hydrogen from the intermediately formed propene molecule [11-18]. It was recently suggested that these elements could intervene directly in the reaction mechanism [19, 20]. M1 phases containing Bi cations, instead of Te and Sb cations, have been synthesized. However, the resulting catalysts appear to be less active when tested for the ammoxidation of propane [21]. This was explained by the Bi content obtained in the synthesized phase, which was lower than that of the M1 phases including Te and Sb cations. Another problem arose with the latter catalysts, for which a structure directing agent was required, which needed to be removed at the end of the synthesis process. This structure directing agent was the ethyl ammonium cation ($EtNH_3^+$) that positions itself in the heptagonal channel, promoting crystallization of the phase, and preventing the channels from being occupied by bismuth cations. The latter effect would be detrimental to the catalytic reaction, since the sites activating the propane C-H bonds, located mainly at the edges of these channels, would become inaccessible.

Following the same reasoning, which led to the study of the substitution of antimony and tellurium by bismuth, it was decided to introduce lead into the M1 phase structure. The same positive effect, arising from the basic characteristics of Pb, was expected for the catalytic properties of this phase. Moreover, lead could be present with two different oxidation states, and could contribute to the exchange of electrons and to the redox mechanism. To this end, we investigated various approaches to the design of a new preparation process, based on a microwave-assisted hydrothermal technique, which was recently shown to be efficient for the preparation of mixed oxide catalysts [22, 23]. Furthermore, this technique can be easily and rapidly implemented, and could be used to support phases on macro-cellular silicon carbide (SiC) foams [24, 25]. It was chosen to introduce other elements with lone pair electrons, such as Sb and Bi, into the structure, whilst avoiding the use of a sacrificial structure directing agent. The aim in this case was also to determine whether this approach could allow the lone pair cation content of the phases to be enhanced, thus making them more efficient.

The catalytic reactions selected to study the catalytic properties of the new phases are the oxidative dehydrogenation of ethane to ethylene, and the partial oxidation of propane to acrylic acid. The synthesized phases were characterized using various physical techniques. As the Pb-containing M1 phase was synthesized for the first time, its crystalline structure was refined.

2. Experimental

2.1. Synthesis protocol

The M1 phases have been prepared by hydrothermal synthesis assisted by microwaves using as starting materials ammonium heptamolybdate $(NH_4)_6Mo_7O_{24}\cdot 4H_2O$ (Sigma-Aldrich 12054-85-2), hydrated vanadium(IV) sulfate $VOSO_4\cdot xH_2O$ (Sigma-Aldrich 123334-20-3) and either bismuth(III) oxychloride BiOCl (Sigma-Aldrich 7787-59-9), antimony(III) sulfate

$Sb_2(SO_4)_3$ (Sigma-Aldrich 7446-32-4) or lead (II) oxide PbO (Sigma-Aldrich 1317-36-8). Beforehand, the amount of water in the hydrated vanadyl sulfate was determined by thermogravimetric analysis. The initial suspension that contained the metals in a molar ratio Mo/V/A (A = Bi, Pb or Sb) equal to 1/0.25/0.05 were prepared by first dissolving respectively in 400 and 200 mL of distilled water, 1.476 g of $(NH_4)_6Mo_7O_{24}\cdot 4H_2O$ (Mo = 65 mmol) and 3.635 g of hydrated $VOSO_4\cdot 3H_2O$ (V=16.25 mmol). The two aqueous solutions were mixed at ambient temperature and stirred for 10 min, resulting a dark purple solution. Then 0.910 g of $Sb_2(SO_4)_3$ 95% or 0.863 g of BiOCl 98% or 0.725 g of PbO (Sb, Bi, Pb = 3.25 mmol) were added to the mixture. The pH of the mixed solution was reduced to 2.0 by adding concentrated H_2SO_4. The 650 mL solution was poured into the 1 L-Teflon vessel of a Milestone's SYNTHWAVE device (Fig. S1). Before starting the heat treatment, dissolved oxygen was removed by bubbling nitrogen for 10 min through the solution. The solution was heated in 10 min to 200°C and maintained at this temperature for 30 min under stirring (600 rpm) and then cooled down to 70°C. The resulting solid was isolated by centrifugation and washed to remove unreacted BiOCl, PbO and minor parasite phases such as M2 or $PbMoO_4$. The washing was performed at 60°C with 10 % hydrogen peroxide aqueous solution for M1(Sb) and with 1.2M hydrochloric acid aqueous solution for M1(Bi) and M1(Pb) (1g of solid for 25 mL of peroxide or acid solution) [26]. The material was finally dried in air at 80°C and calcined under 100 $mL.min^{-1}$ of nitrogen flow for 2 h at 400°C.

The same M1 phases have also been prepared with the aforementioned procedure but using structuring agents in order to see if they could help to the formation of the nanopores, locating at the heptagonal channels and thus improving the phase purity or crystallinity. For that purpose, various potential molybdenum precursors incorporating these agents have been prepared and introduced in place of the standard precursor in the starting solutions. These compounds like ethylamine trimolybdate (EATM) $(CH_3CH_2NH_3)_2Mo_3O_{10}$ or dimethylamine trimolybdate (DMATM) $(CH_3)_2NH_2)_2Mo_3O_{10}.H_2O$ were synthesized as described in the literature [21].

2.2. Characterization of the catalysts

Crystal structure of the synthesized phase samples was characterized by X-ray diffraction (XRD) using a Brüker D5005 diffractometer and Cu-Kα radiation. The powder patterns were collected between 5 and 80° (2θ) with 1s counting time per step of 0.02°2θ and analyzed by Rietveld method using TOPAS 3.0. For the structure determination of the M1 phase containing Pb a powder pattern has been recorded on the large angular range (8-80) with a longer counting time per step (2s). The metal contents of the solids were determined by atomic absorption (ICP) in Argon plasma with a SPECTROLAME-ICP spectrometer and their specific surface area using the BET method. A FEI TITAN ETEM G2 80-300 KV equipped with an objective Cs aberration corrector and an energy-dispersive X-ray (EDX) analyzer (SDD X-Max 80mm^2 from Oxford Instruments^{TM}) has been used for the observation of the catalysts and local elemental chemical analyses. STEM images were acquired on a dark field detector with a camera length of 160 mm corresponding to a collection angles in the range from 45-200 mrad. The sample preparation technique developed for the study of M1 phase has been described previously [27].

X-ray photoelectron spectroscopy (XPS) measurements were performed using a KRATOS Axis Ultra DLD spectrometer. The base pressure in the analysis chamber was better than 1.33 10^{-7} Pa. XPS spectra were measured at 90° (normal angle with respect to the plane of the surface) using a monochromated Al Kα X-ray source with a pass energy of 20 eV. Binding energies were corrected relative to the carbon 1 s signal at 284.6 eV. The signal intensities were measured using integrated areas under the detected peaks. The experimental precision on XPS quantitative measurements was considered to lead to precision on the calculated cationic ratio of 0.10. Coupled thermal and thermogravimetric analyses were performed with a thermobalance TGASTARE from Mettler Toledo. Around 6 mg of sample was heated under air at a rate of 10°C.min^{-1} up to 500°C. Infra-red spectra of the samples prepared using a structural agent, before and after heat-treatment were recorded on an Agilent CARY 630 Instrument at room

temperature. 1-15 mg of sample were characterized and spectra were recorded using 128 averaged scans with a resolution of 4 cm^{-1}. The wavelength varied from 650 to 4000 cm^{-1}. Air spectra were referenced to the blank grid, and absorbance spectra were referenced to the sample with subtracted background. X-Ray Absorption Near Edge Structure (XANES) analyses were performed at the SOLEIL synchrotron on the ROCK beamline (Rocking Optics for Chemical Kinetics) [28]. Spectra at V K-edge (5465.1 eV) were recorded at room temperature in transmission mode. Samples were diluted in boron nitride powder to optimize the absorption jump and pressed into pellets. The analysis of spectra at V K-edge was based on the observations of the pre-edge and edge positions considering the center of mass and the total area of V pre-edge calculated using XANDA Dactyloscope and OriginLab softwares as described before [29]. Pure metal V sample was used to calibrate energy.

Temperature-programmed desorption (TPD) of NH_3 and CO_2 have been used to measure the amount of acidic and basic sites and their distribution in strength. The thermo-desorption apparatus was a BELCAT-M instrument from BEL JAPAN with TCD detection. For NH_3-TPD, the catalysts were first heated from room temperature at 10°C.min^{-1} and kept at 400°C for 10 min, under a 50 ml.min^{-1} flow of helium. A mixture of 1%Vol of Ammonia in helium was then passed over the solid at 200°C with a flow of 50 ml.min^{-1} during 30 min, followed by flushing with helium during 30 min. The desorption of ammonia was finally recorded under the same flow from 200 to 500°C, with a temperature ramp of 5°C.min^{-1}. CO_2-TPD was carried out under the same conditions, except for the adsorption step, made at room temperature.

2.3. Catalytic testing

The catalysts have been tested for the oxidation of propane to acrylic acid and the oxidative dehydrogenation of ethane to ethylene. Both reactions were performed in a fixed bed reactor operating at atmospheric pressure. The catalytic properties were determined between 320 and 420°C with a catalyst amount varying from 0.5 to 1g. Experiments of propane

oxidation were performed with a GHSV (Gas hour space velocity) varying of 3600 h^{-1}. Water was fed and vaporized with an inert gas flow to the reactor using a BRONKHORST controlled evaporator mixer system. The composition of the reactant flow was O_2:C_3H_8: N_2/He: H_2O= 5:10:40:45. The condensable reaction products (acrolein, acrylic acid, acetic acid and acetaldehyde) were trapped in two in-series abatement devices containing acetonitrile and maintained at 0-2°C and analyzed off line using gas chromatographs equipped with FID detectors and a MS 5A (10m x 0.32mm x 12µm) column or a PLOT Q (8m x 0.32mm x 10µm) column. The gas products (propane, propene, CO and CO_2) were analyzed online, using a gas chromatograph**.** The oxidative dehydrogenation of ethane has also been studied at atmospheric pressure using the same method and conditions as previously described [30]. The feedstock composition was O_2:C_2H_6: N_2/He = 10:10:80. Ethane and gas products (ethylene, CO and CO_2) were analyzed with an on-line gas chromatograph. The catalytic tests were carried out for 24 h. No deactivation or selectivity variation was observed during this period and carbon balance were always better than 98%.

3. Results

The X-ray diffraction patterns of Pb-, Bi- and Sb-containing M1 phases, prepared using the new technique and in the absence of a structure directing agent, are presented in Fig. 1. All minor phases observed in the as-prepared solids were completely dissolved during the washing and the final heat treatment at 400°C following this washing strongly improved their crystallinity (Fig. S2). The resulting phases appeared to be highly crystallized and their X-ray patterns correspond well to the ICSD file for the Sb-containing phase (04-017-3606) and to the published one for Bi [21]. The computed cell parameters are very similar, and appear to increase slightly with the size of the lone pair element (Table 1).

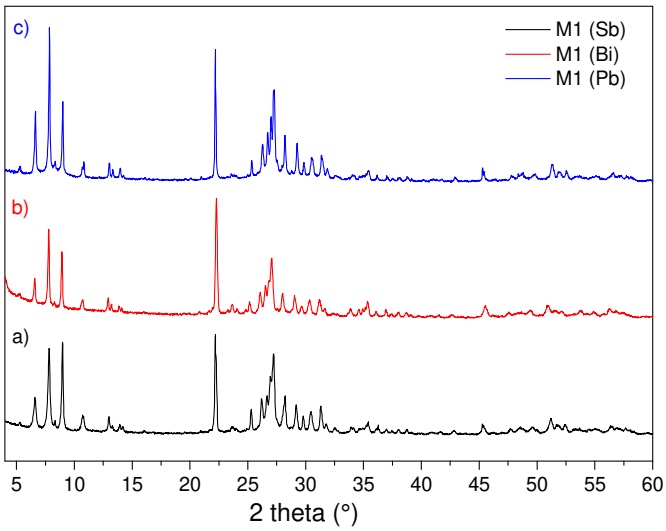

Fig. 1 : X-ray diffraction patterns of the M1(Pb) a), M1(Bi) b), M1(Sb) c) samples synthesized in the absence of a structure directing agent.

Table 1: Cell parameters computed from the X-ray diffraction patterns of synthesized samples, with the cationic ratios computed from the results of chemical and EDX analyses, as well as BET specific surface area (SSA) measurements.

Phase	Cell parameters			Chemical analysis		EDX		SSA
	a (Å)	b (Å)	c (Å)	V/Mo	A/Mo	V/Mo	A/Mo	($m^2.g^{-1}$)
M1(Pb)	21.0626 (8)	26.478 (1)	4.0017 (1)	0.41	0.03	0.54	0.04	18.8
M1(Bi)	21.050 (1)	26.446 (1)	4.0017 (2)	0.44	0.02	0.42	0.03	15.6
M1(Sb)	21.093 (1)	26.554 (2)	3.9988 (3)	0.35	0.10	0.36	0.06	10.9

Both chemical and EDX data showed that the Mo content of the phases was lower than the starting content, which leads to a V/Mo ratio higher than expected. The lone pair elements content is also lower than expected in particular for Bi and Pb. Such feature had previously been observed for Bi and not explained [21]. It is possible that the lacks of elements may be linked to the formation of the minor phases dissolved after synthesis.

The cell parameters computed for the Pb, Bi and Sb phases are very similar, and relatively well-matched with previously published data [3,21,31]. The parameters *a* and *b* appear to decrease with the size of the lone pair [32] whereas *c* parameter does not vary. The specific surface areas

of the solids range between 10 and 20 $m^2.g^{-1}$, as is the case for most specific surface areas reported in the literature, whatever the method used to synthesize them. The results derived from chemical analyses are in good agreement with those estimated by STEM-EDX. The V/Mo ratios were systematically higher than those expected, whereas the A/Mo ratios (A=Sb, Pb, Bi) were lower. Attempts to increase the latter ratios, by adding larger amounts of bismuth or lead precursors, or other precursors, were unsuccessful.

On the other hand, and although the phases could be obtained only through the use of ammonium cations as the structure directing agent, the influence of different structure directing agents on microwave-assisted synthesis was also studied. Several MoVPbO compounds were prepared, while adjusting the reaction conditions and adding other structure directing agents to improve the phase pure purity and avoiding final washing of the samples. Nevertheless, in all cases, side-phases were detected, the phase crystallinity was not substantially improved, and the elemental composition was similar (Table S1).

The three mixed oxides, crystallized with a prismatic morphology, have already been described by numerous authors for other types of M1 phase, and are characterized by a high length/diameter ratio of the rod-shaped particles [33-35]. Figure 2 shows representative SEM images of the M1(Pb) particles. The length axis has been shown to correspond to the [001] direction. In some cases, the 2 to 8 nm length nanorods are agglomerated and interlocked. As a consequence of the high aspect ratio of the material, the exposed surface area is composed of mainly lateral surface planes.

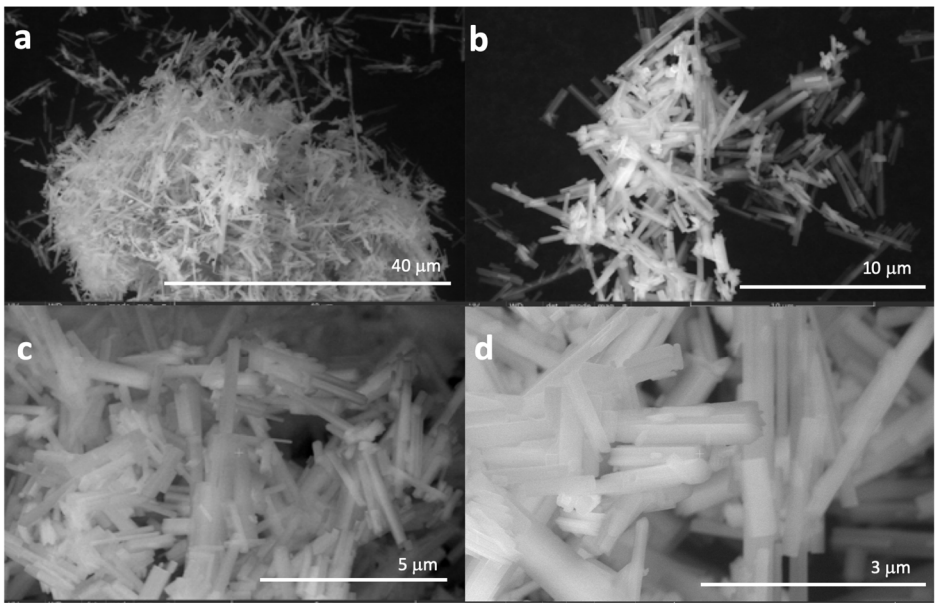

Fig. 2 : SEM images of the M1(Pb) phase at different magnitudes.

The washed phases were characterized before and after heat treatment at 400°C, using infrared spectroscopy, and produced comparable spectra. The spectrum of M1(Pb) is shown in Fig. S3. Over the range between 1000 and 2000 cm^{-1}, the band at 1610 cm^{-1} was assigned to water, whereas the band at 1409 cm^{-1} was assigned to NH_4^+ cations, originating from the metal precursor salts [36]. Below 1000 cm^{-1}, all of the spectra were characterized by a band at 910 cm^{-1}, which was attributed to V–O, and by bands between 874 and 652 cm^{-1}, attributed to Mo–O–Mo [37, 38]. The spectrum of the solid that was heat-treated in air at 400 °C contained the same bands at low frequencies, as well as a band at 1610 cm^{-1}, showing that it had re-adsorbed water from the ambient air after heat treatment. The band at 1409 cm^{-1} disappeared due to decomposition of the ammonium cations (Fig. S3). TG-DTA analyses performed on the M1(Pb) phase, before and after heat treatment, confirmed the infra-red results. Indeed, they showed two weight loss (Fig. 3a). The first of these, observed between 25 and 225°C, is attributed to a loss of water, whereas the second event observed between 250 and 325°C is attributed to the formation of ammonia from NH_4^+. Following the heat treatment of the solid,

further analysis revealed the loss of the same amount of water (re-adsorbed from the ambient air) as in the first observation (Fig. 3b).

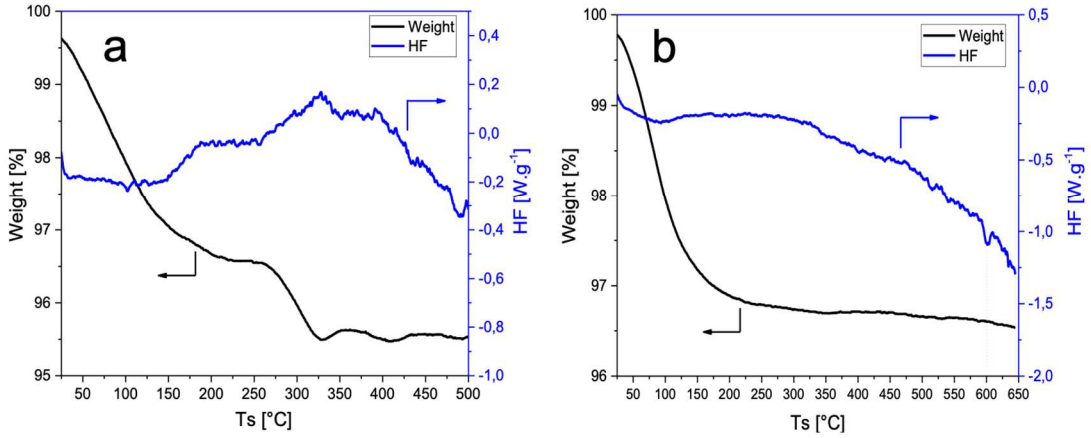

Fig. 3 : TG-DTA curves of MoVPbO recorded (a) after washing and heat treatment at 500°C; after storage in air (b).

In view of the chemical analyses performed and the TG data, the following formula is proposed for the synthesized phase: $Pb_{0.2}(NH_4)_{0.8}Mo_7V_3O_{28}$, $2.6H_2O$. The ammonium cations share the sites on the hexagonal channels with the Pb cations, filling them completely, whereas water is assumed to be located in the heptagonal channels, as well as on the external surface of the phase.

As the structure of the M1(Pb) phase is reported for the first time in the present study, it was refined as the starting model for the bismuth equivalent. Fig. 4 shows the Rietveld simulation, and the refined crystallographic parameters are listed in Table 2.

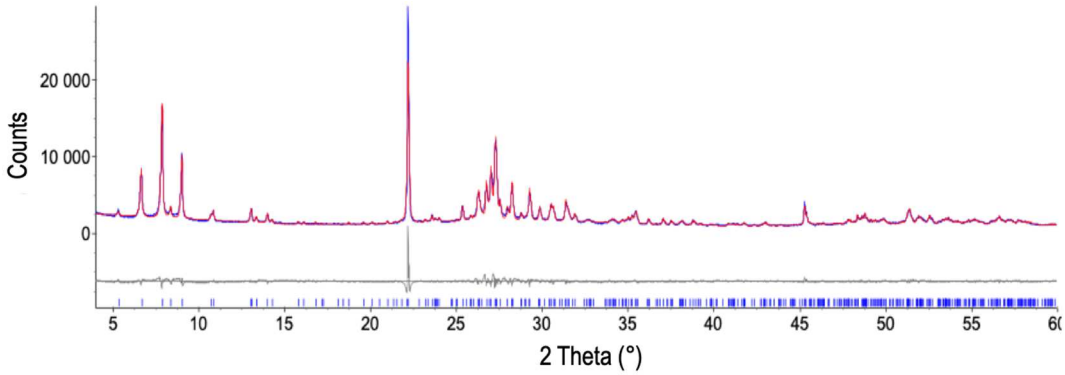

Fig. 4 : Final Rietveld plot for M1(Pb) . The observed data are denoted by a continuous blue line, and the computed one by a red one. The bottom grey line corresponds to the difference curve and the blue marks to the Bragg positions.

The final Rietveld plot is characterized by satisfactory model indicators (Table 2) and the structural model obtained by this refinement shown in Fig. 5, corresponds well to that known for other M1-type orthorhombic phases. The computed atomic coordinates are provided in the form of supplementary data (Table S2). The relative atomic positions of all of the cations were quite close to those of the model developed for bismuth. The refinement shows that Mo and V share all metallic sites, with various extents, with the exception of the M9 site located at the center of the $\{M_6O_{21}\}$ building block, which is occupied by Mo only. After refining the occupancy rates, the following overall formula was established: $Pb_{0.4}Mo_{7.3}V_{2.7}O_{28}$ with the V/Mo and Pb/Mo ratios equal to 0.37 and 0.05, respectively. These ratios are close to those computed from chemical analysis and EDX measurements (Table 1). In the hexagonal channels, the atomic position of the Pb atom appears to be slightly offset from the center of the channels, similarly, although to a lesser extent, to the case of the Sb and Te atoms. All attempts at refinements, involving the addition of an oxygen atom at a reasonable distance in the channels, as in the case of the latter atoms were unsuccessful. This difficulty can easily be explained by the size of the Pb^{2+} cation, when compared to the hexagonal window, and by its inability to adopt a tetrahedral coordination in oxides.

Table 2 : Crystal data and Rietveld refinement parameters.

Empirical formula	$Pb_{0.4}Mo_{7.3}V_{2.7}O_{28}$
M	1314.18
Crystal system	orthorhombic
Space group	Pba2
a (Å)	21.0614(9)
b (Å)	26.4789(12)
c (Å)	4.00161(13)
$\alpha = \beta = \gamma$ (°)	90
V (Å^3)	2231.7(2)
Z	4
λ (Å)	1.5418
No. of structural parameters	136

No of reflections	2440
R_{wp} , R_p, (without background)	0.1128, 0.079
R_{Bragg}	0.034

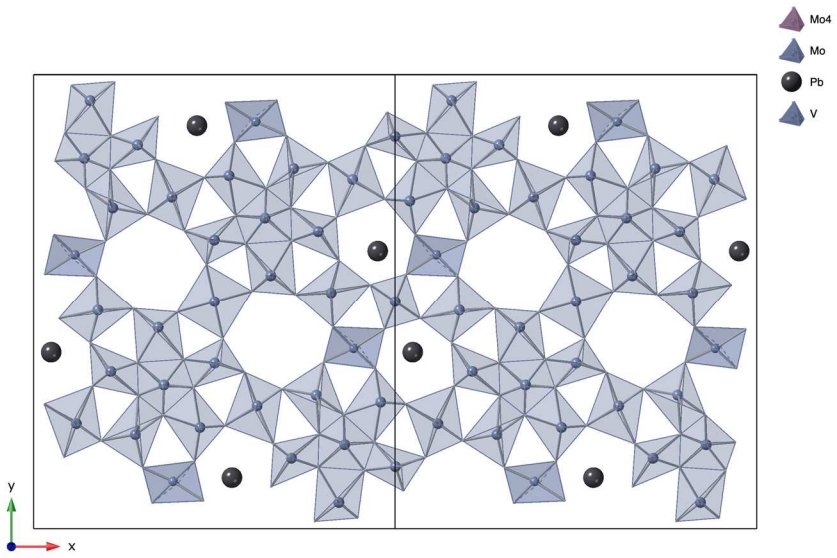

Fig. 5 : Structural diagram of the crystalline orthorhombic M1(Pb) phase along the [001] axis, showing the MO_6 (M=V, Mo) network and the off-centered position of the Pb cations (black spheres) inside the hexagonal channels.

All STEM-HAADF images of the synthesized M1 phases revealed the rod-shaped, crystalline morphology generally encountered with this type of phase This shows that our new preparation process does not produce new types of crystalline texture. STEM-HAADF images of the [001] projections of these phases, corresponding to the rod terminations, are shown in Fig. 6 and Fig. S4.

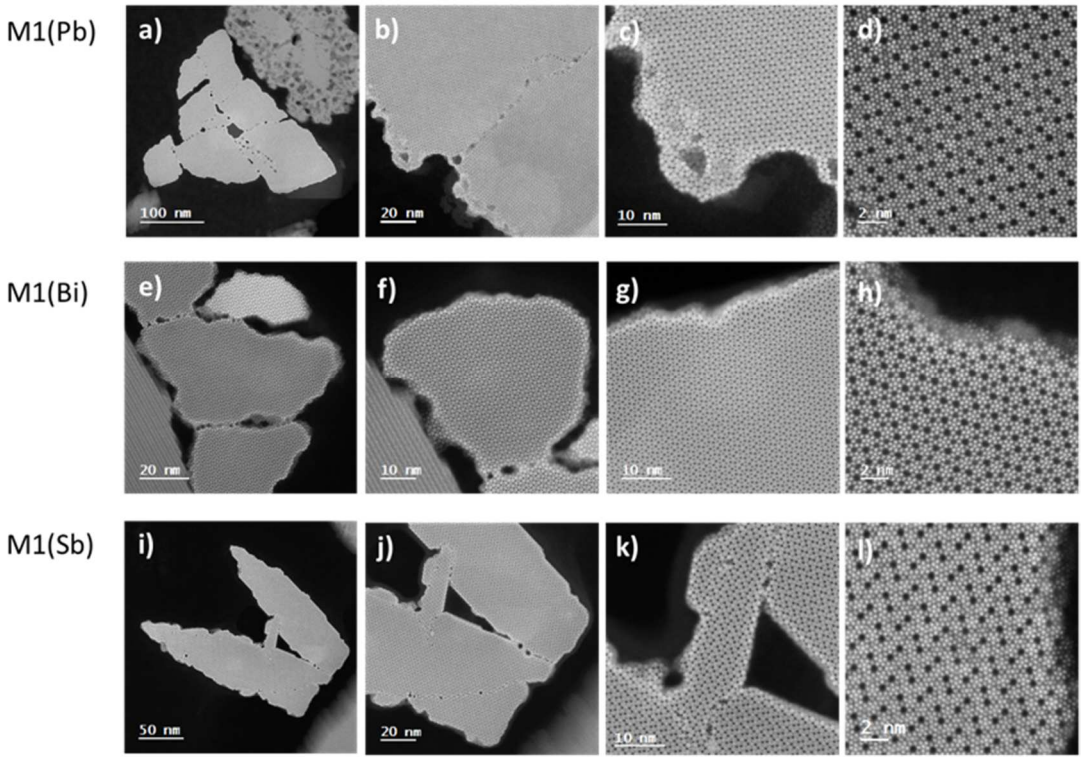

Fig. 6 : Structural diagrams of the crystalline orthorhombic M1(Pb) (from a to d), M1(Bi) (from e to h) and M1(Sb) (from i to l) phases along the [001] axis, showing the channel structure network, as well as systematic decoration of the nanorod borders with columns of $\{Mo_6O_{21}\}$.

These images are similar to those reported in the literature, and reveal large, well-ordered phase domains with no structural defects (Fig. S4). The heptagonal channels appear to be empty; the very weak intensities found in a small number of heptagonal channels were the only point defects that could be identified. The images recorded along the [001] axis also show that the lateral acets of the M1 phase are systematically composed of columns of $\{(Mo)Mo_5\}$ or $\{Mo_6O_{21}\}$, with the staking of units made up from a central, MoO_7 pentagonal bipyramid, sharing edges with five surrounding MoO_6 octahedra (Fig. 6). Similar observations were first reported by Pyrz et al. [39] for the case of M1(Te) phases, and were later confirmed by Aouine et al. [40]. It has been proposed that the formation of these decorative columns is thermodynamically and kinetically preferable to the self-nucleation of other phases [41].

EDX analyses performed during the STEM study are well correlated with chemical and XRD data, and confirm that the hexagonal channels (sites S12) are only partially occupied by lone

pair cations (Table 1). The computed occupation levels are approximately 40, 26 and 64% for Pb, Bi and Sb, respectively. Similar sub-stoichiometries have already been reported for Sb and Bi phases, prepared using other methods. This suggests that the sub-stoichiometry of the phases is not related to their method of preparation. In order to study the influence of the sub-stoichiometry on the local distribution of lone-pair elements, intensity profiles between heptagonal pores, aligned across the S3-S1-S2-S12-S3 site sequence, were analyzed in detail. This type of site sequence was first studied by Blom et al., in order to reveal thermal displacements in corner- and edge-shared cation-oxygen octahedra [41]. The profiles were analyzed after background subtraction, normalization with respect to the intensity maximum, and fitting of the data with a least-squares regression algorithm developed for the analysis of similar profiles in Te-containing M1 phases [40]. This approach allowed the displacements in S12 peak positions, corresponding to the lone-pair cation position in the hexagonal channels, to be measured, and allowed the ratio between the intensities of the peaks, corresponding to the relative occupancy of two coupled S12 sites, to be determined. The accuracy achieved on these parameters is approximately 0.03 nm and 0.10 nm, respectively. The results presented in Fig. 7 and Table 3 show that the Bi cations are positioned at the center of the channels, whereas the Pb and Sb cations, similarly to the Te cations, are slightly off-centered towards the S2 sites. These observations are in good agreement with the structural data obtained for Bi-, Sb- and Te-containing phases, and with the results obtained in study of Pb [3,21,31]. Indeed, the smaller the size of the cationic element, the greater the eccentricity of its location (Fig. S4). This could be explained by the need to optimize oxygen bonding and valence-shell electron pair repulsion, or by the presence of labile oxygen bound to the Te and Sb cations.

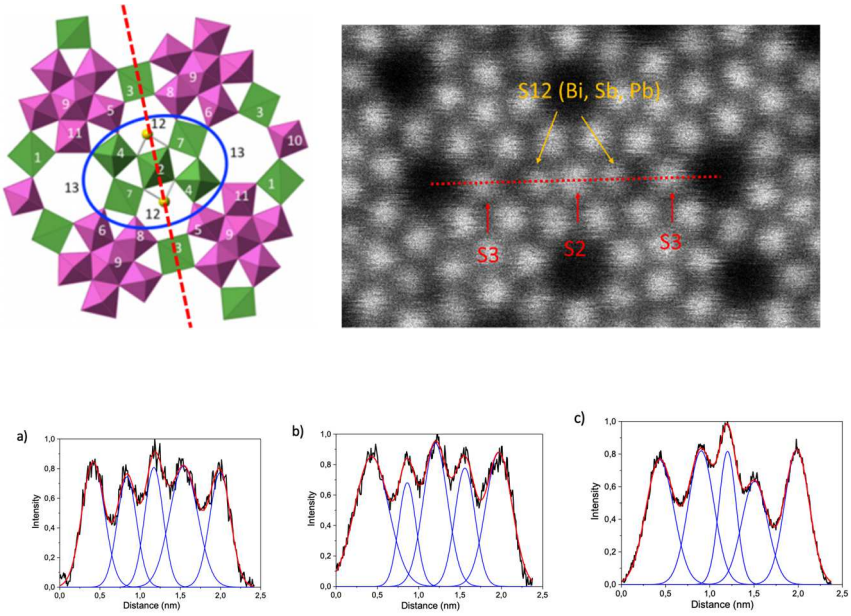

Fig. 7 : Line scan profiles between heptagonal pores, across the S3-S12-S2-S12-S3 site sequence of M1 phases, together with the fitted profiles, for the M1(Pb) a), M1(Bi) b) and M1(Sb) c) phases.

Table 3 : Results for three different M1 phases, of the least-squares regression of average line scans, taken across S3-S12-S2-S12-S3 site sequences between nearby heptagonal pores.

Catalyst	Distance ratio $\frac{S12a - S2}{S3 - S2}$	Distance ratio $\frac{S12b - S2}{S3 - S2}$	Relative intensity of coupled S12 peaks I_{S12a}/I_{S12b}
M1(Bi)	0.52	0.49	1.07
M1(Sb)	0.39	0.39	1.50
M1(Pb)	0.44	0.45	1.10

Although the intensities of the two S3 peaks in each profile are always very similar, the intensities of the two S12 peaks differ, depending on the nature of the lone electron pair element occupying them. The I_{S12a}/I_{S12b} ratio is approximately 1.1 ± 0.1 for Bi and Pb, but is equal to 1.5 ± 0.1 for Sb (Table 3). Similar results have been reported for Te, with an I_{S12a}/I_{S12b} ratio close to 1.5 [40]. No periodicity was observed in the respective arrangements of the two types of site, within the structures, and both associated sites were found to fill up in a totally random fashion. At the time of writing, we have still no clear explanation for this phenomenon. However, it is interesting to note that a difference in intensity is found for the phases containing Sb and Te

only, for which the heptagonal channels are occupied not only by cations with lone pairs of electrons, but also by infinite, oxygen-forming defective chains [42]. It is possible that in these cases, the charge balance in the structure is influenced locally, not only by changing the number of cations, but also by the number of oxygen atoms, with oxidation state modifications being possible for Te and Sb, but not for other elements. Such a property could influence the filling of two neighboring channels, and lead to different relative intensities.

It has long been known that M1 phases can contain vanadium with two different degrees of oxidation [43, 44]. In the context of the present study, it was important to determine the average degree of vanadium oxidation in the prepared phases. Figure 8 shows the XANES spectra, following background subtraction and normalization at the V K-edge. The pre-edge centroïd position and the parameters of the vanadium oxidation state are listed in Table 4.

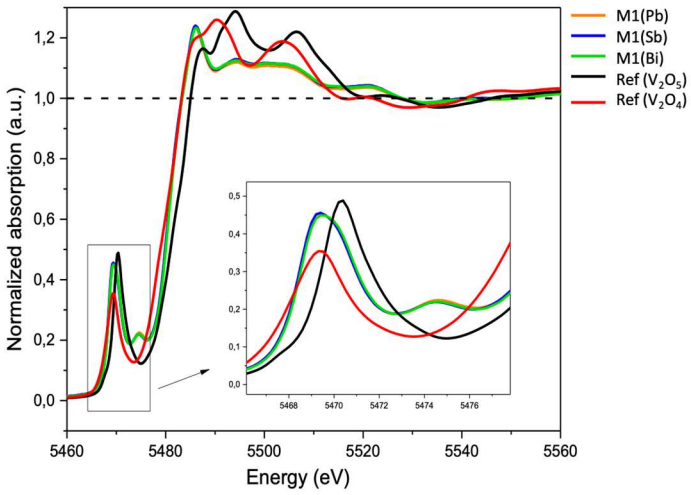

Fig. 8: Vanadium K-edge XANES spectra, showing the details of pre-edge absorption of the various samples, synthesized using the microwave-assisted technique.

Table 4: Energy position of the edge and computed mean oxidation state of vanadium, determined from the V K-edge XANES spectra for three different M1 phases.

Sample	Pre-edge peak centroid position (eV)	Mean V oxidation state
M1(Pb)	5469.64	4.27
M1(Sb)	5469.63	4.26
M1 (Bi)	5469.69	4.32

We note that the average vanadium oxidation state of the M1 phases is slightly greater than that generally reported in previous studies (approximately 4.2 ± 0.1), for M1 phases prepared using other methods. This higher oxidation state could be explained by the need to counterbalance the charge defect related to the lower lone-pair element content of the phases prepared using the microwave-assisted technique. Considering the +2 and +6 oxidation states for Pb and Mo, respectively, together with the chemical composition of the M1(Pb) phase, the computed mean oxidation state of vanadium would be equal to +4.23. This is close to the value of +4.27 computed from XAS data.

Prior to catalytic testing, it was important to verify whether or not the surface and bulk compositions were similar like for the Sb containing phase, which was analyzed before [34]. The Pb- and Bi-containing phases were characterized using X-ray electron spectroscopy. The spectra obtained showed that the surface cation ratios were again comparable to those of the bulk material except for the vanadium surface content which was slightly lower (Table 5). Both V^{4+} and V^{5+} are identified at the surface of the phases (Fig. S5). Their relative content is similar to that of the bulk material for M1(Pb), with a corresponding mean oxidation of 4.27, and a

slightly higher value around 4.44 in the case of M1(Sb) and M1(Bi). Contrarily to what is often observed on this type of phase, Mo appeared systematically present at the surface only as a single spin-orbit Mo3d doublet attributed to Mo^{6+} (Fig. S6). Bi and Pb peaks were attributed to Bi^{3+} and Pb^{2+} from peak positions reported in NIST Database [45] or XPS Handbook [46] and by comparison with results of recent publications [47, 48]. It can be specified that in the case of lead a single doublet with symmetrical peaks at 138.60 and 143.50 eV, which excludes the possible presence of Pb^{4+} for which the Pb $4f_{7/2}$-$4f_{5/2}$ core-level are at lower energies close to that of the Pb-metal and would lead to be an asymmetry in the line-shape of the observed signal [48]. As regard to Sb element, it was present as Sb^{5+} and Sb^{3+} with a relative cationic ratio comparable to that observed previously [49].

Table 5 : Surface elementary ratios of the cations of the three different M1 phases from XPS analysis data.

Compound	Element	M/Mo	oxidation state	Binding energy (eV)	% oxidation state
M1(Sb)	Sb (3d)	0.14	Sb^{5+}	531.22 540.56	60 % Sb^{5+}
			Sb^{5+}	530.54 539.88	40 % Sb^{3+}
	Mo (3d)	1	Mo^{6+}	232.91 236.03	100 % Mo^{6+}
	V (2p)	0.27	V^{4+}	516.37 523.77	55 % V^{4+}
			V^{5+}	517.20 524.60	45% V^{5+}
M1(Pb)	Pb (4f)	0.03	Pb^{2+}	138.60 143.50	100 % Pb^{2+}
	Mo (3d)	1	Mo^{6+}	232.60 235.75	100 % Mo^{6+}
	V (2p)	0.29	V^{4+}	516.32 523.74	73 % V^{4+}
			V^{5+}	517.26 524.81	27% V^{5+}
M1(Bi)	Bi (4f)	0.02	Bi^{3+}	159.20 164.50	100 % Bi^{3+}
	Mo (3d5/3)	1	Mo^{6+}	232.41 235.55	100 % Mo^{6+}
	V (2p)	0.32	V^{4+}	516.04 523.42	56 % V^{4+}
			V^{5+}	516.97 524.46	44% V^{5+}

The synthesized phases were tested as catalysts for the simple oxidative dehydrogenation of ethane, which makes it possible to assess their activity in the oxidation of light alkanes in general. First, the results obtained with the M1(Bi) phase were compared with those obtained by Ishikawa et al. on a similar phase, which was synthesized using a different technique, but tested under the same conditions [21] (Fig. 9).

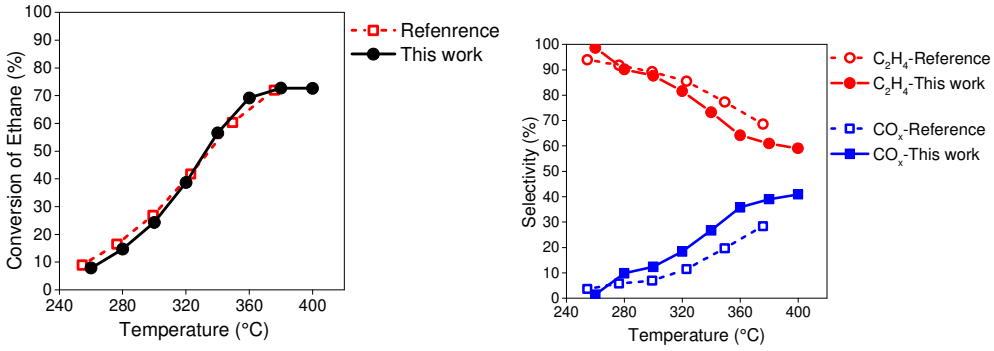

Fig. 9 : Conversion and selectivity variations as a function of temperature, over M1(Bi) synthesized using the microwave-assisted technique, and over a similar, previously reported reference phase [21]. Mass of catalyst = 0.5 g; $C_2H_6/O_2/N_2$ = 1/1/8; feed gas flow rate = 50 mL.min^{-1}

The results obtained on both solids are comparable, thus confirming that the test apparatus and method were valid, and showing that the new synthesis process described here does not lead to any structural or compositional modification of the solids. The Bi-, Sb- and Pb-containing phases were then compared as catalysts for the same reaction (Fig. 10). The Pb- and Sb-containing phases appeared to be slightly less active than the Bi-containing phase, but were more selective to ethylene, so that very similar acrolein yields were obtained with the three catalysts. This is understandable because, as has previously been shown by studies of catalysts containing tellurium and antimony, or bismuth and no cations, the lone-pair element does not intervene in the activation of the alkanes, which is the limiting step of the reaction [18, 21]. These results also confirm that the heptagonal channels of all the structures were indeed empty, since if they had been occupied, active sites located on the edges of these channels would not have been accessible, and the conversion rate would have been close to zero.

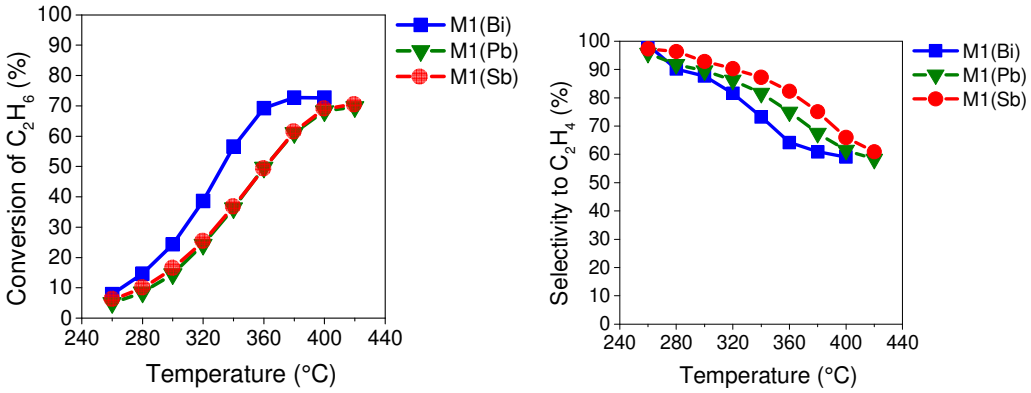

Fig. 10 : Conversion rate and selectivity to ethylene as a function of temperature, for different M1 phases, using the same catalyst mass, under the same test conditions: catalyst mass = 0.5 g, feed gas flow rate = 50 mL.min^{-1}, composition $C_2H_6/O_2/N_2$ = 1/1/8.

The lone-pair element did not influence the ethylene selectivity as it appeared when the selectivity to ethylene is plotted as a function of ethane conversion at 360°C, for each of the three different M1 phases (Fig. S7). This chart clearly shows that the same selectivity-conversion curve is well matched to the data recorded for all three catalysts.

The M1(Pb) and M1(Sb) phases were also tested as catalysts for the oxidation of propane to acrylic acid. In this case, the M1(Sb) was used as a reference, for which the results obtained by Ivars et al. provide a benchmark for comparison purposes [50]. The catalysts used were relatively similar in terms of composition and texture, and the catalytic reaction conditions were rather similar.

Table 6 : Oxidation of propane over M1(Sb)-based catalysts at 380°C, feed gas flow rate = 60 mL.min^{-1} with a composition $C_3H_8/O_2/H_2O/N_2$ = 5/10/45/40, contact time GHSV = 3600 h^{-1}.

Catalyst	Propane conversion (%)	Acrylic acid (AA)	C_3H_6	Acetic acid (AceA)	CO	CO_2	Acetone
M1(Sb)	20	49	15	11	13	11	1
Ref. M1(Sb)[a]	23	56	11	5	13	13	1
M1(Pb)	19	31	15	12	25	17	-

[a] Experimental results reported by [50], contact time W/F = 200 $g_{cat}.h.(mol_{C_3H_8})^{-1}$, $C_3H_8/O_2/H_2O/N_2$ = 4/8/58/30. AA: acrylic acid, AceA: acetic acid.

The results provided in Table 6 show that the catalytic properties of the synthesized M1(Sb) are rather similar, although they are slightly lower than the best performances reported in the literature. The fact that compatible activities were obtained for solids again indicates that, although the lone-pair electron cations are not involved in the activation of the alkane molecules (as has been proposed by some authors, they contribute mainly to the dehydrogenation of the intermediately formed alkene molecules. The new M1(Pb) phase appears to be almost as active as the other catalysts, but considerably less selective to acrylic acid. This loss of selectivity is compensated by a higher selectivity to CO and CO_2, rather than to propene. This could be explained by the presence of Pb rather than Sb, which affects the acid-base properties of the catalyst.

Temperature-programmed desorption of ammonia and CO_2 (NH_3-TPD and CO_2-TPD) was used to measure oxide surface acidity and basicity and to assess the presence of any direct correlation between their acid-base and catalytic characteristics. The NH_3-TPD profiles obtained on the various phases are shown in Figure 11, with the measured quantities of surface-area-normalized desorbed NH_3.

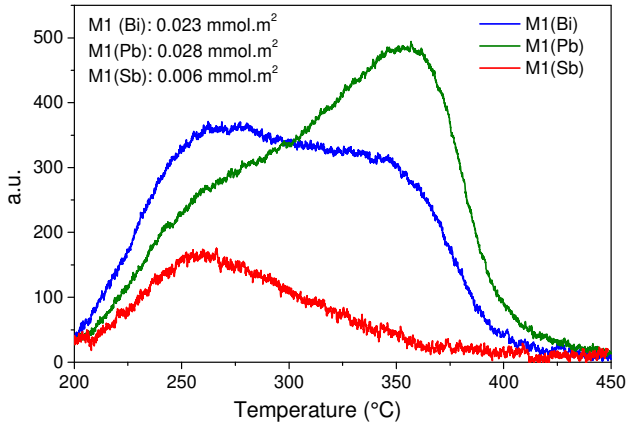

Fig. 11: NH_3-TPD profiles of the M1(Bi) M1(Pb) and M1(Sb) catalysts.

Adsorbed ammonia desorbs between 180 and 400°C similarly to other crystalline M1 phases [51-53]. Two desorption temperature ranges with maxima between 260 and 270°C and 340 and

350°C are defined, allowing the sites to be classified as either weak to medium, or strong acid sites, respectively. The acidity of the three M1 phases decreased in the order M1(Pb)>M1(Bi)>>M1(Sb) both in terms of strength and number of sites. The M1(Sb) exhibits only weak to medium sites whereas the two other phases show large amounts of strong acid sites. Temperature-programmed desorption of CO_2 was used to characterize the basicity of the solids. However, no peaks were detected with this experiment. To account for sensitivity issues, we used a similar setup with a mass spectrometer as desorbed molecules detector but the same result was obtained. This allowed to conclude that basic sites are not numerous and are weak.

We have seen that the activity of M1(Pb) and M1(Sb) phases are almost the same which indicated that the acidity does not affect the propane activation, which should also be the case for ethane oxidation. Similar feature was reported when putting in relation the acidic and catalytic properties of M1(Sb) and M1(Te) phases containing or not Nb [54]. In the same study, a correlation between the selectivity of the catalysts and their acidity was observed, the less selective been the more acidic. This was explained by the preferential occurrence of the mechanism with carbonium ion formation on acid center that would operate in the transformation of propene [55]. This would result in the formation of propoxide type adsorption complexes, which decompose in the presence of water to produce isopropyl alcohol that easily dehydrogenated on redox centers leading to acetone and further to CO and CO_2. The same explanation may be retained in this case study also in agreement with other studies [49]. Finally, the relative similarity in acidic properties between M1(Bi) and M1(Pb) and catalytic properties in ethane oxidative dehydrogenation suggests that comparable high catalytic properties and efficiency could also be observed in the ammoxidation of propane. Finally, it is worth mentioning that the crystal structure of the catalysts was preserved after catalytic reactions. Unlike catalysts containing Te, their total composition was also maintained [56].

4. Conclusion

In the present study, vanado-molybdate phases with an M1 type of bronze structure were successfully obtained, using microwave-assisted hydrothermal synthesis. Besides considerably shortening the reaction time from 48 h to 10 min, and lowering the energy required for the reaction, this technique makes it possible to dispense with the use of a structure directing agent, which is expensive and must be removed by means of post-synthesis treatment. Well-crystalized and pure Sb-, Bi- and Pb-containing phases were prepared.

As an M1 phase containing Pb was not previously reported, the structure of this phase is described in the present study: it is found to be well matched with the structural model of an M1-type phase, with Pb atoms located inside hexagonal channel, in a slightly off-centered position. The relative occupancy of vanadium and molybdenum on the octahedral positions, and of Bi in the channels, are in good agreement with the characterizations obtained through the use of analytical or spectroscopic techniques. For the three synthesized phases, STEM-HAADF analysis confirms the absence of extended structural defects and the presence of $\{Mo_6O_{21}\}$ columns, connected to each other by one octahedron only on the facets of the nanorods. This analysis also shows that the Bi or Pb cation occupancy levels of two neighboring S12 sites are similar, but systematically different from those associated with Te and Sb.

The prepared catalysts were tested for the oxidative dehydrogenation of ethane and the oxidation of propane. The synthesized phases appeared to be as active as the corresponding phases, prepared using other methods. The introduction of Sb, Bi or Pb had only a small effect on the catalytic activity in both reactions. A marked decrease in selectivity to acrylic acid was observed only on the Pb-containing phase, which occurred to the benefit of that in carbon oxides, in the mild oxidation of propane. This decrease in selectivity is ascribed to an increase in surface acidity. One could also postulate that the similarity between Bi and Pb-containing M1 phases in terms of catalytic properties in the tested reactions and surface acidity leads to a comparable efficiency of the two phases in the ammoxidation of propane.

5. Acknowledgments

XANES spectroscopy characterization was made at Soleil Synchrotron was supported by a public grant overseen by the French National Research Agency (ANR) as part of the "Investissements d'Avenir" program (reference: ANR10-EQPX45).

6. References

[1] M. Hatano, K. Kayou, Europeen Process for Producing Nitriles, Eur. Patent 318,295 A1, 1988 attributed to Mitsubishi Kasei Corp.

[2] T. Ushikubo, K. Oshima, A. Kayou, M. Hatano, Ammoxidation of propane over Mo-V-Nb-Te mixed metal oxide catalysts in: C. Li, Q. Xin (Eds.), Study of Surface Science and Catalysis, Elsevier, Amsterdam, 121, 1997, p. 473.

[3] P.Jr. DeSanto, D.J. Buttrey, R.K. Grasselli, C.G. Lugmair, A.F.Volpe, B.H. Toby, T. Vogt, Structural aspects of the M1 and M2 phases in MoVTeNbO propane ammoxidation catalysts, Z. Kristallogr. Cryst. Mater. 219 (2004) 152-165.

[4] H. Murayama, D. Vitry, W. Ueda, G. Fuchs, M. Anne, J.L. Dubois, Structure characterization of orthorhombic phase in MoVTeNbO catalyst by powder X-ray diffraction and XANES Appl. Catal. A: Gen. 318 (2007) 137-142.

[5] R.K. Grasselli, D.J. Buttrey, J.D. Burrington, A. Andersson, J. Holmberg, W. Ueda, J. Kubo, C.G. Lugmair, A.F. Volpe Jr, Active centers, catalytic behavior, symbiosis and redox properties of MoV(Nb,Ta)TeO ammoxidation catalysts, Top. Catal. 38 (2006) 7-16.

[6] P. Concepcion, S. Hernandez, J.M. Lopez Nieto, On the nature of active sites in MoVTeO and MoVTeNbO catalysts: The influence of catalyst activation temperature, Appl. Catal. A: Gen. 391 (2011) 92-101.

[7] T. Lunkenbein, L. Masliuk, M. Plodinec, G. Algara-Siller, S. Jung, M. Jastak, P. Kube, A. Trunschke and R. Schlögl, Structural Complexity in Heterogeneous Catalysis: Cataloging Local Nano-Structures Site specific and localized structural displacements in open structured multimetallic oxides, Nanoscale, 12 (2020) 6759-6766.

[8] X. Tu, M. Niwa, A. Arano, Y. Kimat, E. Okazaki, S. Nomura, Controlled silylation of MoVTeNb mixed oxide catalyst for the selective oxidation of propane to acrylic acid, Appl. Catal. A : Gen. 549 (2018) 152-160.

[9] B. Deniau, J.M.M. Millet, S. Loridant, N. Christin, J.L. Dubois Effect of several cationic substitutions in the *M1* active phase of the MoVTeNbO catalysts used for the oxidation of propane to acrylic acid, J. Catal. 260 (2008) 30-36.

[10] C. Qiu, C. Chen, S. Ishikawa, T. Murayama, W. Ueda, Crystalline Mo-V–W-mixed Oxide with Orthorhombic and Trigonal Structures as Highly Efficient Oxidation Catalysts of Acrolein to Acrylic Acid, Top. Catal. 57 (2014) 1163-1170.

[11] R.K. Grasselli , J.D. Burrington , D. J. Buttrey , P. DeSanto Jr. , C.G. Lugmair , A.F. Volpe Jr. , and T. Weingand, Catalysts: Multifunctionality of active centers in (amm)oxidation from Bi-Mo-O_X to Mo-V-Nb-(Te,Sb)-O_x, Top. Catal. 23 (2003) 5-22.

[12] R.K. Grasselli, C.G. Lugmair, A.F. Volpe Jr., Towards an Understanding of the Reaction Pathways in Propane Ammoxidation Based on the Distribution of Elements at the Active Centers of the M1 Phase of the MoV(Nb,Ta)TeO System, Top. Catal. 54 (2011) 595-604.

[13] A.C. Sanfiz, T.W. Hansen, D. Teschner, P. Schnörch, F. Girgsdies, A. Trunschke, R. Schlögl, M. Hong Looi, and S. Bee Abd Hamid, Dynamics of the MoVTeNb Oxide M1 Phase in Propane Oxidation, J. Phys. Chem. C 114 (2010) 1912-1921.

[14] E.V. Ishchenk, T.Yu. Kardash, R.V. Gulyaev, A.V. Ishchenko, V.I. Sobolev, V.M. Bondareva, effect of K and Bi doping on the M1 phase in MoVTeNbO catalysts for ethane oxidative conversion to ethylene, Appl. Catal. A: Gen. 514 (2016) 1-13.

[15] J. Woo, V.V. Guliants, QSTEM-based HAADF-STEM image analysis of Mo/V distribution in MoVTeTaO M1 phase and their correlations with surface reactivity, Appl. Catal. A: Gen. 512 (2016) 27-35.

[16] A. “Bean” Getsoian, V. Shapovalov and A.T. Bell, DFT+U Investigation of Propene Oxidation over Bismuth Molybdate: Active Sites, Reaction Intermediates, and the Role of Bismuth, J. Phys. Chem. C 117 (2013) 7123-7137.

[17] T. Vogt, D.A. Blom, L. Jones, D.J. Buttrey, ADF-STEM Imaging of Nascent Phases and Extended Disorder Within the Mo–V–Nb–Te–O Catalyst System, Top. Catal. 59 (2016) 1489-1495.

[18] B. Deniau, T.T. Nguyen, P. Delichere, O. Safonova, J.M.M. Millet, Redox State Dynamics at the Surface of MoVTe(Sb)NbO M1 Phase in Selective Oxidation of Light Alkanes, Top. Catal. 56 (2013) 1952-1962.

[19] Y. Zhu, P.V Sushko, D. Melzer, E. Jensen, L. Kovarik, C. Ophus, M. Sanchez-Sanchez, J.A. Lercher, and N.D. Browning, Formation of Oxygen Radical Sites on MoVNbTeOx by Cooperative Electron Redistribution, J. Am. Chem. Soc. 139 (2017) 12342-12345.

[20] J.M. Arce-Ramos, G. Rugg, A. Genest, N. Rösch, Probing the Positions of TeO Moieties in the Channels of the MoVNbTeO M1 Catalyst: A Density Functional Theory Model Study, Catal. Lett. (2021) *DOI:* 10.1007/s10562-021-03538-3

[21] S. Ishikawa, Y. Goto, Y. Kawahara, S. Inukai, N. Hiyoshi, N.F. Dummer, T. Murayama, A. Yoshida, M. Sadakane and W. Ueda, Synthesis of Crystalline Microporous Mo-V-Bi Oxide for Selective (Amm)Oxidation of Light Alkanes, Chem. Mater. 29 (2017) 2939-2950.

[22] G. Hidalgo, M. Tonelli, L. Burel, M. Aouine, J.M.M. Millet, Microwave-assisted hydrothermal synthesis, characterization and catalytic performance of $Fe_2(MoO_4)_3$ in the selective oxidation of propene, Catal. Today 363 (2021) 36-44.

[23] T.M.N. Le, N. Guillou, M. Aouine, J.M.M. Millet, β(L)-$Bi_2Mo_2O_9$ a new bismuth molybdate highly active and selective mild oxidation catalyst J. Catal. in press (2021).

[24] X. Ou, S. Xu, J.M. Warnett, S.M. Holmes, A. Zaheer, A.A. Garforth, M.A. Williams, Y. Jiao, X. Fan, Creating hierarchies promptly: Microwave-accelerated synthesis of ZSM-5 zeolites on macrocellular silicon carbide (SiC) foams, Chem. Eng. J. 312 (2017) 1-9.

[25] T.T. Nguyen, L. Burel, D.L. Nguyen, J.M.M. Millet, Catalytic performance of MoVTeNbO catalyst supported on SiC foam in oxidative dehydrogenation of ethane and ammoxidation of propane, Appl. Catal. A: Gen. 433 (2012) 41-48.

[26] B. Deniau, G. Bergeret, B. Jouguet, J.L. Dubois, J.M.M. Millet, Preparation of Single M1 Phase MoVTe(Sb)NbO Catalyst: Study of the Effect of M2 Phase Dissolution on the Structure and Catalytic Properties, Top. Catal. 50 (2008) 33-42.

[27] T. Epicier, M. Aouine, T.T. Nguyen, and J.M.M. Millet, Spatial Distribution of the Vanadium Atomic Species in MoVTeO and MoVTeNbO Oxide Catalysts as Revealed by High-Angle Annular Dark-Field Scanning Transmission Electron Microscopy, ChemCatChem, 9 (2017) 3526-3533.

[28] https://www.synchrotron-soleil.fr/fr/lignes-de-lumiere/rock

[29] O.V. Safonova, B. Deniau, J.M.M. Millet, XANES study of Sb, V and Mo cations at L_1 and K edges in the MoVTe(Sb)NbO Catalysts for Oxidation of Propane and electrical conductivity measurements *in operando* conditions, J. Phys. Chem. B 110 (2006) 23962-23967.

[30] T.T. Nguyen, M. Aouine, J.M.M. Millet, Optimizing the efficiency of MoVTeNbO catalysts for ethane oxidative dehydrogenation to ethylene, Catal. Comm. 21 (2012) 22-26.

[31] M. Sadakane, K. Yamagata, K. Kodato, K. Endo, K. Toriumi, Y. Ozawa, T. Ozeki, T. Nagai, Y. Matsui, N. Sakaguchi, W. D. Pyrz, D. J. Buttrey, D. A. Blom, T. Vogt, W. Ueda, Synthesis of Orthorhombic Mo-V-Sb-O by Assembly of Pentagonal Mo_6O_{21} Polyoxometalate Building Blocks, Angew. Chem. Int. Ed. 48 (2009) 3782-3786.

[32] D. Hamani, O. Masson and P. Thomas, Localization and steric effect of the lone electron pair of the tellurium Te^{4+} cation and other cations of the p-block elements. A systematic study, J. Appl. Cryst. 53 (2020) 1243-1251.

[33] D. Vitry, Y. Morikawa, J.L. Dubois, W. Ueda, Mo-V-Te-(Nb)-O mixed metal oxides prepared by hydrothermal synthesis for catalytic selective oxidations of propane and propene to acrylic acid, Appl. Catal. A: Gen. 251 (2003) 411-424.

[34] M. Baca, J.M.M. Millet, Bulk oxidation state of the different cationic elements in the MoVTe(Sb)NbO catalysts for oxidation or ammoxidation of propane Appl. Catal A: Gen. 279 (2005) 67-77.

[35] N.R. Shiju, V.V. Guliants, Recent developments in catalysis using nanostructured materials, Chem. Appl. Catal. A: Gen. 356 (2009) 1-17.

[36] S. Ishikawa, T. Murayama, S. Ohmura, M. Sadakane, W. Ueda, Synthesis of Novel Orthorhombic Mo and V Based Complex Oxides Coordinating Alkylammonium Cation in Its Heptagonal Channel and Their Application as a Catalyst, Chem. Mater. 25 (2013) 2211-2219.

[37] P. Botella, P. Concepcion J.M. Lopez Nieto, B. Solsona, Effect of Potassium Doping on the Catalytic Behavior of Mo–V–Sb Mixed Oxide Catalysts in the Oxidation of Propane to Acrylic Acid, Catal. Lett. 89 (2003) 249-253.

[38] S.C. Su, A.T. Bell, A Study of the Structure of Vanadium Oxide Dispersed on Zirconia, J. Phys. Chem. B 102 (1998) 7000-7007.

[39] W.D. Pyrz, D. A. Blom, N.R. Shiju, V. V. Guliants, T. Vogt, D.J. Buttrey, The effect of Nb or Ta substitution into the M1 phase of the MoV(Nb,Ta)TeO selective oxidation catalyst, Catal. Today 142 (2009) 320-328.

[40] M. Aouine, T. Epicier, J.M.M. Millet, In Situ Environmental STEM Study of the MoVTe Oxide M1 Phase Catalysts for Ethane Oxidative Dehydrogenation, ACS Catal. 6 (2016) 4775-478.

[41] D.A. Blom, T. Vogt, L.F. Allard, D.J. Buttrey, Observation of Sublattice Disordering of the Catalytic Sites in a Complex Mo-V-Nb-Te-O Oxidation Catalyst Using High Temperature STEM Imaging, Top. Catal. 57 (2014) 1138-1144.

[42] J.M.M. Millet, M. Baca, A. Pigamo, D. Vitry, W. Ueda, J.L. Dubois, Study of the valence state and coordination of antimony in MoVSbO catalysts determined by XANES and EXAFS, Appl. Catal. A: Gen. 244 (2003) 359-370.

[43] P. DeSanto Jr., D.J. Buttrey, R.K. Grasselli, C.G. Lugmair, A.F. Volpe, B.H. Toby, T. Vogt, Structural characterization of the orthorhombic phase M1 in MoVNbTeO propane ammoxidation catalyst, Top. Catal. 23 (2003) 23-38.

[44] M. Baca, J.M.M. Millet, Bulk oxidation state of the different cationic elements in the MoVTe(Sb)NbO catalysts for oxidation or ammoxidation of propane, Appl. Catal. A: Gen. 279 (2005) 67-77.

[45] NIST X-Ray Photoelectron Database, Version 4.1, National Institute of Standards and Technology, Gaithersburg, 2012.

[46] J.F. Moulder, W.F. Stickle, P.E. Sobol, K.D. Bomben, Handbook of X-Ray Photoelectron Spectroscopy, Physical Electronics Inc., Eden Prairie, 1995.

[47] H. Hou, L. Wang, F. Gao, X. Yang and W. Yang, $BiVO_4$@TiO_2 core–shell hybrid mesoporous nanofibers towards efficient visible-light-driven photocatalytic hydrogen production, J. Mater. Chem. C, 7, 2019, 7858-7864.

[48] D.A. Zatsepin, D.W. Boukhvalov, N.V. Gavrilov, E.Z. Kurmaev, A.F. Zatsepin, L. Cui, V. Ya. Shur, A.A. Esin, XPS-and-DFT analyses of the Pb4f-Zn3s and Pb5d-O2s overlapped ambiguity contributions to the final electronic structure of bulk and thin-film Pb-modulated zincite, Appl. Surf. Sci. 405 (2017) 129-136.

[49] F. Ivars-Barceló, J.M.M. Millet, T. Blasco, P. Concepción, J.S. Valente, J.M. López Nieto Understanding effects of activation-treatments in K-free and K-MoVSbO bronze catalysts for propane partial oxidation, Catal. Today 238 (2014) 41-48.

[50] F. Ivars, B. Solsona, E. Rodríguez-Castellon, J.M. Lopez Nieto, Selective propane oxidation over MoVSbO catalysts. On the preparation, characterization and catalytic behavior of M1 phase, J. Catal. 262 (2009) 35-43.

[51] S. Ishikawa, D. Kobayashi, 7. Konya, S. Ohmura, T. Murayama, N.Yasuda, M. Sadakane, W. Ueda, Redox Treatment of Orthorhombic $Mo_{29}V_{11}O_{112}$ and Relationships between Crystal

Structure, Microporosity and Catalytic Performance for Selective Oxidation of Ethane. J. Phys. Chem. C 119 (2015) 7195-7206.

[52] T.V. Andrushkevich, G.Y. Popova, Yu.A. Chesalov, E.V. Ischenko, M.I. Khramov, V.V. Kaichev, Propane ammoxidation on Bi promoted $MoVTeNbO_x$ oxide catalysts: Effect of reaction mixture composition, Appl. Catal. A: Gen. 506 (2015) 109-117.

[53] R. Quintana-Solórzano, Isidro Mejía-Centeno, Hector Armendáriz-Herrera, Joel Ramírez-Salgado, Andrea Rodríguez-Hernandez, Maria de Lourdes Guzman-Castillo, Jose M. Lopez Nieto, and Jaime S. Valente, Discerning the Metal Doping Effect on Surface Redox and Acidic Properties in a $MoVTeNbO_x$ for Propa(e)ne Oxidation, https://doi.org/10.1021/acsomega.1c01591.

[54] M. Baca, A. Pigamo, J.L. Dubois, J.M.M. Millet, Fourier transform infrared spectroscopic study of surface acidity by pyridine adsorption on the M1 active phase of the MoVTe(Sb)NbO catalysts used in propane oxidation, Catal. Comm. 6 (2005) 215-220.

[55] Y. Moro-oka, Y. Takita, A. Ozaki, Catalytic oxidation of olefin over oxide catalysts containing molybdenum: I. Product distribution in propylene oxidation over the cobalt-molybdenum system, J. Catal. 12 (1968) 291-297.

[56] J.S. Valente, H. Armendaŕiz-Herrera, R. Quintana-Solorźano, P. Ángel, N. Nava, A. Masso and J.M. Lopẽz Nieto, Chemical, Structural, and Morphological Changes of a MoVTeNb Catalyst during Oxidative Dehydrogenation of Ethane, ACS Catal. 4 (2014) 1292-1301.

FIGURES CAPTION

Fig. 1: X-ray diffraction patterns of the M1(Pb) a), M1(Bi) b), M1(Sb) c) samples synthesized in the absence of a structure directing agent.

Fig. 2: SEM images of the M1(Pb) phase at different magnitudes.

Fig. 3: TG-DTA curves of MoVPbO recorded (a) after washing and heat treatment at 500°C; after storage in air (b).

Fig. 4: Final Rietveld plot for M1(Pb). The observed data are denoted by a continuous blue line, and the computed ones by a red one. The bottom grey line corresponds to the difference curve and the blue marks to the Bragg positions.

Fig. 5: Structural diagram of the crystalline orthorhombic M1(Pb) phase along the [001] axis, showing the MO_6 (M=V, Mo) network and the off-centered position of the Pb cations (black spheres) inside the hexagonal channels.

Fig. 6: Structural diagrams of the crystalline orthorhombic M1(Pb) phase along the [001] axis, showing the channel structure network, as well as systematic decoration of the nanorod borders with columns of $\{Mo_6O_{21}\}$.

Fig. 7: Line scan profiles between heptagonal pores, across the S3-S12-S2-S12-S3 site sequence of M1 phases, together with the fitted profiles, for the M1(Pb) a), M1(Bi) b) and M1(Sb) c) phases.

Fig. 8: Vanadium K-edge XANES spectra, showing the details of pre-edge absorption of the various samples, synthesized using the microwave-assisted technique.

Fig. 9: Conversion and selectivity variations as a function of temperature, over M1(Bi) synthesized using the microwave-assisted technique, and over a similar, previously reported reference phase [21]. Mass of catalyst = 0.5 g; $C_2H_6/O_2/N_2$ = 1/1/8; feed gas flow rate = 50 mL.min^{-1}

Fig. 10: Conversion rate and selectivity to ethylene as a function of temperature, for different M1 phases, using the same catalyst mass, under the same test conditions: catalyst mass = 0.5 g, feed gas flow rate = 50 mL.min^{-1}, composition $C_2H_6/O_2/N_2$ = 1/1/8.

Fig. 11: NH_3-TPD profiles of the M1(Bi) M1(Pb) and M1(Sb) catalysts.